Materials Transactions, Vol. 51, No. 10 (2010) pp. 1861 to 1870

Vertical and Horizontal Directional Solidification of Zn-Al and Zn-Ag Diluted Alloys

Sergio F. Gueijman[1], Carlos E. Schvezov[1,2] and Alicia E. Ares[1,2,*]

[1]*School of Science, National University of Misiones, 1552 Félix de Azara Street, 3300 Posadas-Misiones, Argentina*
[2]*National Science Research Council of Argentina (CONICET), de Buenos Aires, Argentina*

Zinc-Aluminum and Zinc-Silver alloys were solidified in horizontal and vertical form and the results obtained analyzed. Thermal parameters such as the cooling rates, the liquidus and solidus interphase velocities, and the temperature gradients were determined. The velocity of the liquidus interphase is greater than or sometimes equal to the velocity of the solidus interphase. In the vertical setup, columnar-to-equiaxed (CET) grain transition was obtained. CET does not occur in the horizontal one-directional solidification when critical minimum gradients reach values greater than 0.1 K/mm. [doi:10.2320/matertrans.M2010036]

(Received February 1, 2010; Accepted July 20, 2010; Published September 25, 2010)

Keywords: *vertical directional solidification, horizontal directional solidification, columnar-to-equiaxed transition, zinc-aluminum alloys, zinc-silver alloys*

1. Introduction

Alloys directionally solidified exhibit structures in form of columnar grains that often finalize with an equiaxed zone. In these cases the phenomenon of the CET has occurred.[1)] In the last decades a great deal of effort has been devoted to the understanding of the mechanism behind the development of the CET during solidification because the grain structure influences the mechanical properties of the castings.

Particularly, the experimental work carried out to understand the interaction between the parameters implied in transitions from the columnar structure to the equiaxed structure, in different alloy systems, has been based on the determination of superheat, fluid flow, cooling rate, temperature gradients, supercooling, mechanical disturbance, inoculation, the addition of grain refiner and casting size.[2–4)]

Zinc-Aluminum (ZA) alloys have been of great interest in past decades due to their structural applications and microstructural behavior. Its controversial phase diagram is still under study. Since the 1970's, the Zn-Al systems have been studied by adding copper in order to transform the properties of these materials and are thus no longer considered as materials without an added value. More recently, silver has been incorporated into Zn-Al alloys in order to replace the copper metal initially studied, and a superplastic behavior has been found under certain conditions. Also, these alloys show good resistance to corrosion in some environments.[5,6)]

Unfortunately, these alloys are susceptible to porosity defects which occur at the bottom of the alloys that are called underside shrinkage. These defects add up production costs in ZA alloys because they generate a surface defect at the bottom. The work performed by M. Sahoo *et al.* indicate that the underside shrinkage can be completely eliminated by placing coolers and adding different elements of group I and II.[7)]

These authors studied the CET grain transition in previous research using only different vertical solidification devices.[8–10)] In the present work, we aim to contribute to a better understanding of the phenomenon of directional solidification by comparing the results of vertical and horizontal directional solidification of three diluted Zinc-Aluminum alloys and two Zinc-Silver alloys, by analyzing and comparing the influence of their thermal parameters such as cooling rates, thermal gradients and velocities of the liquidus and solidus interphases.

In the particular case of the interphase velocities, it is necessary to clarify that in the present research we tracked the moving interphases using thermocouple measurements, and did not track dendrite tips, since temperature measurements are determined from a small volume and not a surface. Temperature measurements were used to track averaged [liquid/(solid + liquid)] interphases, namely [L/(S + L)] (or I_L interphases), [(liquid + solid)/(eutectic + solid)] interphases, namely [(S + L)/(E + L)] (or I_E interphases) and [(solid + liquid)/solid], namely [(S + L)/S] interphases (or I_S interphases) but not solid/liquid "interfaces", so dendrite tip surfaces, or equiaxed grain surfaces may be in any solid + liquid region (see Fig. 1).

It is assumed here that solid can not exist beyond the [L/(S + L)] interphase and that liquid can not exist beyond the [(S + L)/S] interphase. It is only into the mushy (solid + liquid) zone where all the "interfaces" do exist, and the mushy zone is at temperatures between the local liquidus temperature and the local solidus (or eutectic) temperature.

2. Experimental

2.1 Directional solidification

A vertical and a horizontal one-directional solidification devices (Figs. 2 and 3 respectively) were used to perform the experiments with diluted Zinc-Aluminum and Zinc-Silver alloys of chosen compositions. Three diluted Zinc-Aluminum alloys (Zn-1 mass%Al, Zn-2 mass%Al and Zn-5 mass%Al) and two Zinc-Silver alloys (Zn-1 mass%Ag and Zn-2 mass%Ag) were prepared. In the case of the vertical setup, a set of samples of Zn-Al alloys were directionally solidified, using glass cylindrical molds of 22 mm of internal diameter, and cooled predominantly from the bottom, using a

*Corresponding author, E-mail: aares@fceqyn.unam.edu.ar

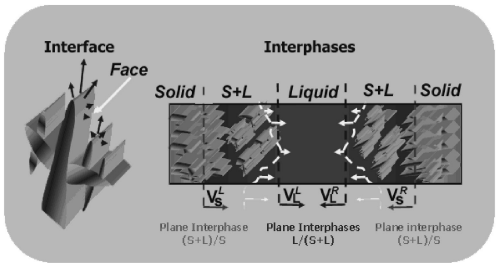

Fig. 1 Scheme showing the dissimilarity between considering interface and interphases.

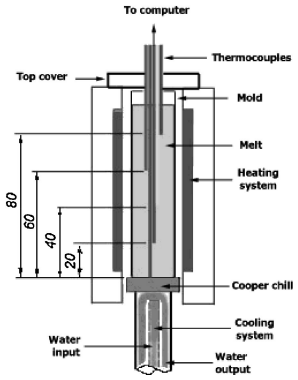

Fig. 2 Experimental set-up used for the vertical one-directional solidification experiments.

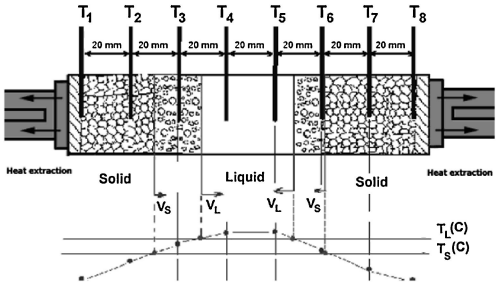

Fig. 3 Experimental setup used for the horizontal one-directional solidification experiments.

tubular heat exchanger device. In the case of the vertical setup, five specimens of Zn-1 mass%Al, two specimens of Zn-2 mass%Al and one specimen of Zn-5 mass%Al were prepared. The experimental setup and techniques are described elsewhere.[8–10] In the vertical solidification, the melt was heated to the required temperature; the heat unit was turned off while cooling water was forced to circulate into the heat extraction system. Temperature measurements were made during solidification using K-Type chromel/alumel thermocouples (1 mm and 1.5 mm stainless steel diameter and 300 mm length) introduced into Pyrex® glass rods of 2.5 mm internal diameter. The vertical distance between adjacent thermocouples was chosen in approximately 20 mm. For the eutectic alloy were utilized hand made K-type thermocouples using thin bare wires isolated with a ceramic compound in a glass envelope (3.15 to 3.25 mm external diameter and 1.8 to 2 mm internal diameter). The whole system was inserted into a bigger Pyrex® tube of ~15 mm external diameter filled with powder graphite. The same distance between thermocouples was kept.

On the other hand, a set of samples of Zn-Ag alloys were directionally solidified in a similar fashion after the preparation of the alloys (one specimen of Zn-1 mass%Ag and one specimen of Zn-2 mass%Ag). In this case, the alloys were prepared by melting Ag and Zn simultaneously in two separate furnaces, and adding the latter (Zn) to the first (Ag). Since the two melting points of the pure elements are too far away and the melting point of Ag is near the boiling point of Zn, the preparation of these alloys was rather difficult and some zinc oxidation occurred, and thus the final composition of the alloy is not fully guaranteed. While Zn was melted in a graphite crucible, Ag was melted in a ceramic crucible, and then they were rapidly mixed together. Since the diffusion of Ag in Zn and vice versa is quite fast, the addition of small quantities of Zn to the Ag lowers the melting point, forming a Ag-rich alloy which is then used as a precursor to prepare the alloy with the final composition. We used pure elements, electrolytic Zn and Ag 99.99%. After preparation, the alloy was cast in a gypsum mold with suitable cylindrical dimensions to be used in the vertical furnace. Subsequently, the set of samples of Zn-Ag alloys were directionally solidified in the vertical setup, using Pyrex® glass cylindrical molds of 22 mm of internal diameter. The length of the samples was around 80 mm. It is noteworthy to point out that the nominal composition of the Zn-Ag alloys do not exceed 2 mass% of Ag and that the melting point of the alloys did not exceed the limiting operating temperature of the Pyrex® mold.

Thermocouples were previously calibrated using Zinc and Aluminum at their melting points. During solidification experiments of Zn-Al alloys, the temperature measured by each thermocouple was recorded at regular intervals of about 1 min. During solidification experiments of Zn-Ag alloys, the temperature measured by each thermocouple was recorded at regular intervals of about 10 s.

In the case of horizontal solidification, ceramic molds of 50 mm in diameter were used for horizontal solidification experiments cooled from both ends. Eight made K-type thermocouples were used in this experimental setup. For the horizontal setup, thermocouples were fabricated with thin chromel-alumel wires of 0.5 mm diameter that were inserted into bifilar ceramics of ~4.0 mm external diameter and ~1.0 mm hollow diameter and introduced inside Pyrex® glass rods of 7.0 mm external diameter and ~5.3 mm internal diameter. Adjacent thermocouples were located at a distance of ~20 mm. Temperatures were measured at regular intervals of 10 s.

A schematic drawing of the horizontal experimental device is shown in Fig. 3. Small 140 mm long hemicylindrical probes of Zn-Al alloy were solidified in the horizontal setup. The heat flux toward the ends of the sample was obtained by two cooling systems located at the ends of the ceramic crucible. In this setup, temperatures at eight different positions were measured using a TC 7003C acquisition system and recorded every 1 min using SensorWatch® software in a compatible PC from the early beginning until the end of the solidification. Alloys were prepared with high purity metals (electrolytic Zinc and commercial grade Aluminum). For the horizontal setup, a set of three specimens were prepared (One specimen of Zn-1 mass%Al and two specimens of Zn-5 mass%Al). The alloy was first melted and mixed in a graphite crucible using a conventional furnace and then poured into a previously heated ceramic crucible. The crucible with the alloy was located into the horizontal furnace and heated up above the melting point of the alloy. The solidification of the sample was obtained by cooling down the alloy using the cooling system which extracts the heat toward both ends (Fig. 3).

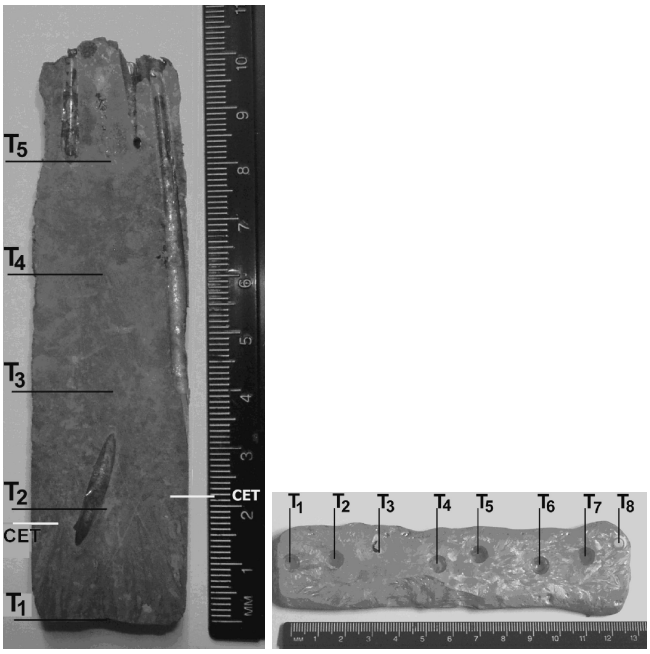

(a) (b)

Fig. 4 (a) Macrostructures of a Zn-1 mass%Al sample vertically solidified. (b) Macrostructure of a Zn-5 mass%Al sample horizontally solidified. The horizontal and vertical lines in the figures indicate the positions of the thermocouples during the experiment.

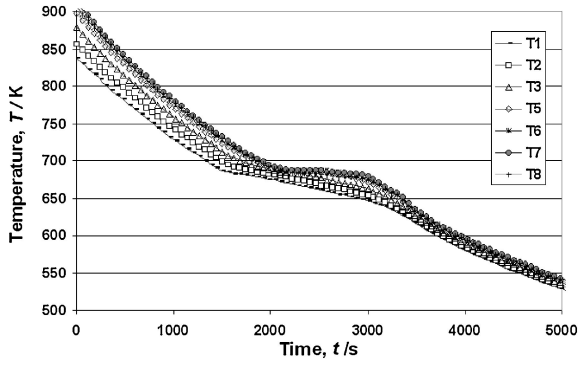

(a)

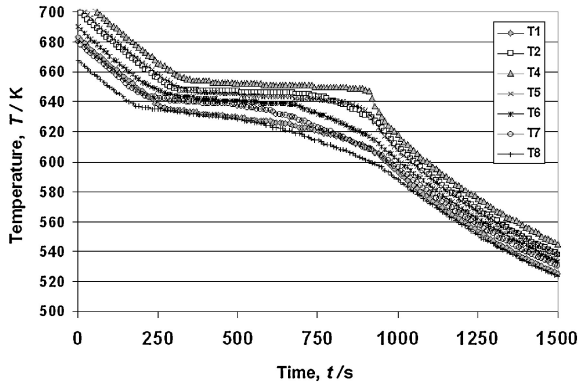

(b)

Fig. 5 Temperature versus time curves for (a) a vertically solidified Zn-1 mass%Al and (b) a horizontally solidified Zn-5 mass%Al samples.

2.2 Metallography

After solidification, both the vertical and horizontal directionally solidified Zn-based alloy samples were cut in the axial direction. The samples were polished and etched using concentrated hydrochloric acid for ~3 s at room temperature, followed by rinsing and wiping off the resulting black deposit. To develop the microstructures, the samples were etched with a mix containing chromic acid (50 g Cr_2O_3; 4 g Na_2SO_4 in 100 ml of water) for 10 s at room temperature.[11] The typical macrostructures of both the vertically solidified Zn-1 mass%Al and the horizontally solidified Zn-5 mass%Al samples are shown in Figs. 4(a) and (b).

The position of the transition in vertically solidified samples was located by visual observation and using an Arcano® optical microscope, and the distance from the chill zone of the sample was measured with a ruler. As reported before, it can be seen in Fig. 4(a) that the CET is not sharp, showing a zone where some equiaxed grains co-exist with columnar grains.

The size of the transition zone is in the order of up to 10 mm. As previously reported,[8–10] no effects of the set of thermocouples in the transition, either acting as nucleating sites or changing the solidification structure, were observed.

The position of the transition in horizontally solidified samples was located by visual observation and the distance from the chill zone of the sample was measured with a ruler. In this case, the thermocouples seem to act sometimes as nucleating sites in the proximities of the glass rods, probably due to the fact that they also behave as a small heat sink, since the glass rods are not immersed in the melt as it happens in the case of the vertical setup.

3. Results and Discussion

3.1 Directional solidification and thermal parameters

In vertical solidification, the CET was obtained in all the experiments. Figure 4(a) shows the CET for the Zn-1 mass%Al alloy. No effects of the set of the thermocouples in the transition either acting as nucleating sites or changing the solidification structure were observed; Figure 4(a) also shows that the transition in grain size is not sharp; there is a "zone" of CET. The smallest diameter of the samples used in the present work produced less fluid flow than in other cases previously reported.[4,6,12–14] In the macrograph of Fig. 4(a) it is also possible to observe the pores and cavities resulting from the contraction.

A typical set of cooling curves is shown in Figs. 5(a) and (b). In the case of vertical solidification, the thermocouple T_1 is at the lowest position and the first to reach the solidification front whereas T_8 is at the highest position. In all the curves it is possible to identify a period corresponding to the cooling of the melt, a second period of solidification and the final period of cooling of the solid to ambient temperature.

In addition, temperature (T) versus time (t) curves were obtained for each running in the horizontal solidification (Fig. 5(b)). The beginning and the end of the solidification in each finite volume were estimated from the change in the slope of the temperature versus time curves, taking the time derivatives of each curve. Each thermocouple characterizes the temperature of the whole volume (approximately 20 mm wide).

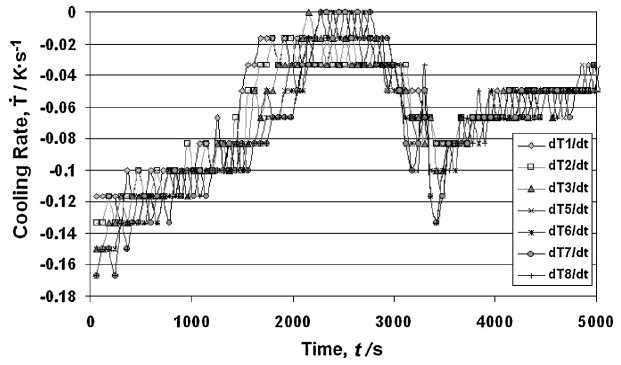

(a)

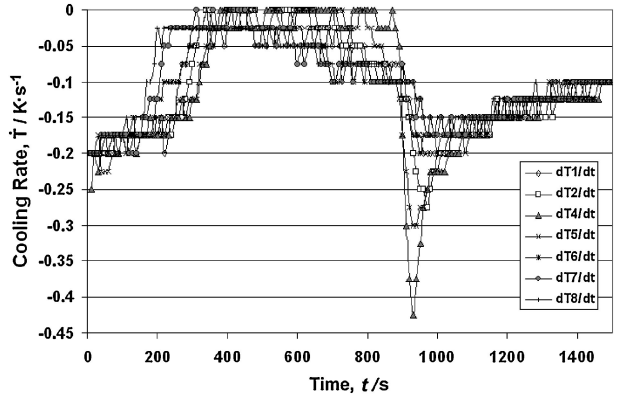

(b)

Fig. 6 Averages cooling rates for (a) a vertically solidified Zn-1 mass%Al and (b) a horizontally solidified Zn-5 mass%Al samples.

In the present research, solidus or eutectic temperatures are considered non-equilibrium temperatures because, during solidification segregation occurs and the local composition of a given volume changes as the solidification progresses, thus changing the local solidus or eutectic temperatures given by the equilibrium diagram for the alloy; however, solidus or final eutectic temperatures are also points since they are the ending of the freezing curve, which is at this "non-equilibrium" temperature during the cooling of the alloy.

Departures from the equilibrium temperature arise also because temperature measurements were carried out under a dynamic regime of cooling rate, and those departures from equilibrium are less when the cooling rate is lower (i.e. near the center of the sample).

3.2 Cooling rate

The cooling rates were determined taking the approximated derivatives with respect to time for each thermocouple position using a central difference numerical technique. The cooling rates in the liquid and in the solid are not constant. This effect occurred for both vertical and horizontal solidification. It is observed that the cooling rate decreases with the sample temperature. This can be seen from the analysis of cooling rates shown in Figs. 6(a) and (b) for the vertically solidified Zn-1 mass%Al and Zn-5 mass%Al alloys, respectively. The rate of change of the cooling rates in the liquid state is faster than the rate of change in the solid state and may be mainly attributed to the higher effective thermal conductivity of the liquid.

Furthermore, changes in the slope of the temperaure vs time curve at the near beginning of solidification of a given volume in the sample occurs by the latent heat released far away of the considered volume, thus changing the solidification conditions of that volume before the alloy's volume undergoes a phase change, in such a manner that the cooling rate before the onset of solidification in a given volume inside the sample is not (and generally should not be) the same as the cooling rate before the onset of solidification in the alloy's volume considered at the extremities of the sample. The cooling rate before the onset of solidification in a given volume inside a sample is generally lower than that near the chilled ends or the mold walls. This fact should be addressed when modeling solidification structures.

3.3 Interphase position, velocity and acceleration

A typical result of the position of the liquidus and eutectic interphases as a function of time is schematically shown in Figs. 7(a) to (f) for different vertically solidified alloys. In the case shown in Figs. 7(a) and (b) there are only two interphases: the liquidus interphase and the solidus interphase, both of which run from the bottom to the top in the case shown in Figs. 7(c) and (d) the solidification is also one-directional but since some heat is lost from the top, a three-interphase system is formed: two interphases are liquidus and run in opposite direction, and one interphase is solidus and runs upward since the heat extraction is predominantly from the bottom. In Figs. 7(e) and (f), it can be noticed the presence of four solidification fronts, two upward and two downward.

The experimental data in Fig. 8(a) for a Zn-1 mass% Al alloy vertically solidified shows the presence of two solidification fronts running in opposite direction, which are two liquidus interphases corresponding to $[L/(S+L)]$ interphases, one ascending and one descending. This figure also shows the presence of another solidification front, the solidus interphase corresponding to the $[(S+L)/S]$ interphase, only ascending. Note that the solidus front increases monotonically in time.

The experimental data in Fig. 8(b) for an Zn-1 mass% Al horizontally solidified sample shows the presence of two solidification fronts running in opposite direction, two liquidus interphases corresponding to $[L/(S+L)]$ interphases, one running from left to right and the other running from right to left. It can also be seen from the figure that there are two solidus interphases corresponding to $[(S+L)/S]$ interphases running in opposite direction, one running from left to right and the other from right to left.

In the case of horizontal solidification, liquidus interphases usually meet near the geometrical center of the probe if the heat extraction is similar from both ends, as shown in Fig. 8(b). In the case of solidus interphases they also meet near the geometrical center of the probe if the heat extraction and the cooling rate are similar at both ends and the mushy zone is nearly homogeneous and isotropic, however, experimental data show that this is not always true. Even though the heat extraction and cooling rates were similar from both ends, the liquidus interphases did not meet at the same geometrical position as the solidus interphases, as it was shown in a previous work.[15] The solidification ended in the

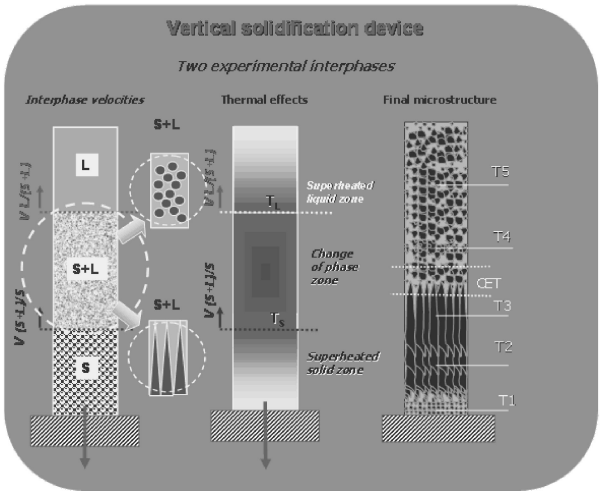

(a)

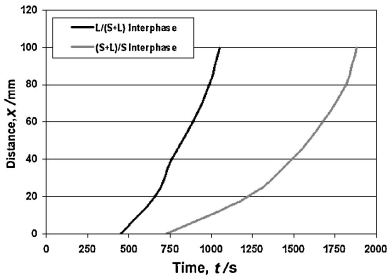

(b)

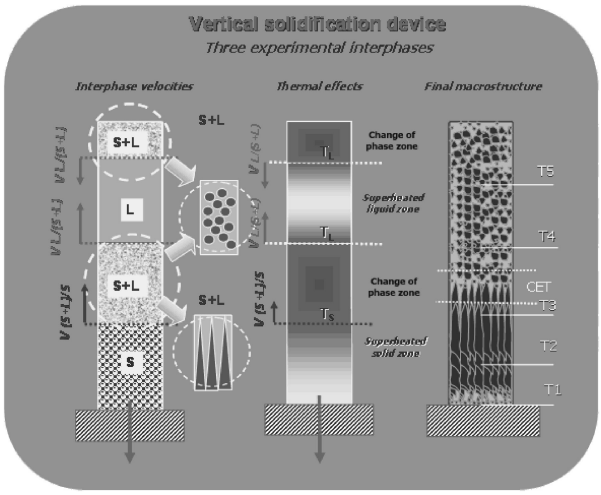

(c)

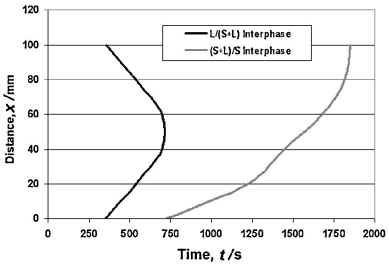

(d)

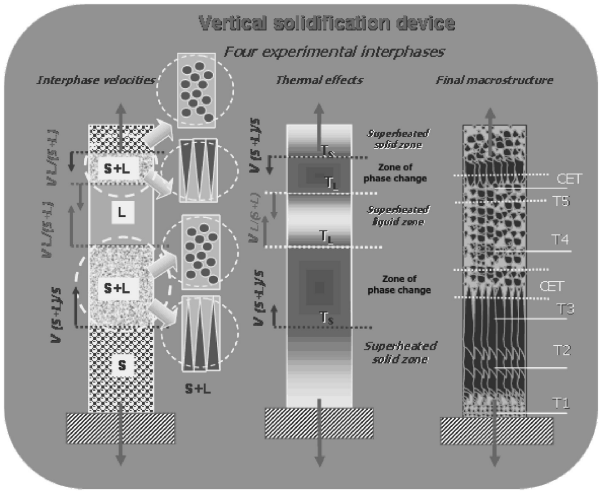

(e)

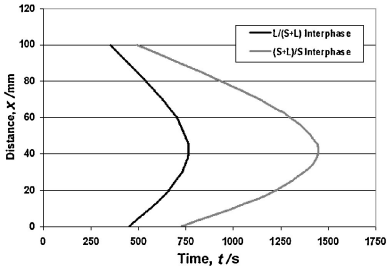

(f)

Fig. 7 Positions of the liquidus and solidus interphases in Zn-Al samples during various conditions of solidification. (a) Vertical directional solidification with two interphases (schematic). (b) Positions of the liquidus (I_L) and solidus (I_S) interphases versus time: the interphase reaches the position of each thermocouple considering only two ascending fronts. (c) Vertical directional solidification with three interphases (schematic). (d) Positions of the liquidus (I_L) and solidus (I_S) interphases versus time: the interphase reaches the position of each thermocouple considering three solidification fronts (two ascending and one descending). (e) Vertical directional solidification with four interphases (schematic). (f) Positions of the liquidus (I_L) and solidus (I_S) interphases versus time: the interphase reaches the position of each thermocouple considering four solidification fronts (two ascending and two descending).

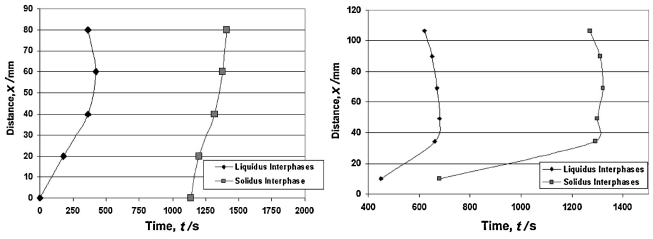

(a) (b)

Fig. 8 Local solidification times for Zn-1%Al alloys. (a) Experimental positions of the liquidus (I_L) and solidus (I_S) interphases for a Zn-1 mass%Al alloy vertically solidified. (b) Local solidification time curves of a Al-1%Zn sample horizontally solidified.

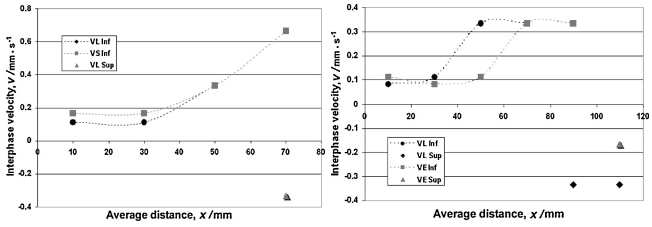

(a) (b)

Fig. 9 Average velocities of the I_L and I_S interphases for different alloys. (a) Zn-1 mass%Al vertically solidified with a system of three interphases. (b) Zn-2 mass%Al vertically solidified with a system of four solidification interphases. Only the experimental averaged liquidus velocity and the final eutectic velocity are shown.

position where the solidus interphases met, i.e., a surface inside the sample.

For alloys showing an eutectic transformation, the velocities of the solidification fronts were calculated as the ratio of the distance between thermocouples and the time taken by any of the solidification interphases (fronts), [L/(S + L)], [(S + L)/(E + L)] and [(L + S)/S] or [(E + L)/S], to move from the lower to the upper thermocouple at the non-equilibrium transformation temperatures T_L^*, T_{Ei}^*, and T_{Ef}^* or T_S^*. These velocities are called velocity of the liquidus front, V_L, velocity of the eutectic front, V_E, or velocity of the solidus front, V_S, respectively. The velocities of all the interphases were experimentally determined as an average velocity in the interval between two adjacent thermocouples whose temperature records were reliable.

For vertical one-directional solidification, the following should be addressed in order to determine the velocities of the interphases:

(1) For Zn-Al alloys with an Al content less than or equal to 1 mass%, if the solidification occurs from the base of the cylinder upward (one-directional vertical solidification upwards) and the position vs. time curves grow monotonically, there are only two solidification interphases, I_L and I_S at temperatures T_L^* and T_S^* (or T_E^*) with two characteristic average velocities, V_L and V_S (or V_E).

(2) For Zn-Al alloys with an Al content greater than 1 mass% but less than or equal to 5 mass%, if the solidification occurs from the base of the cylinder upward (one-directional vertical solidification upwards) and the position vs. time curves grow monotonically, there are only three solidification interphases, I_L, I_E and I_S, running upwards at temperatures T_L^* and T_{Ei}^* and T_{Ef}^* (or T_S^*), with three characteristic average velocities, V_L, V_E and V_S.

(3) Due to segregation, both (1) and (2) can occur in samples solidified in the conditions mentioned above.

(4) For Zn-Al alloys with an Al content less than or equal to 1 mass%, if the solidification occurs predominantly from the base of the cylinder upward (one-directional vertical solidification upwards with heat losses from the top) and the position vs. time curves grow monotonically only for the solidus interphase but not for the liquidus interphase, there are only three solidification interphases, two I_L fronts and one I_S front at temperatures T_L^{*Sup}, T_L^{*Inf} and T_E^* (or T_S^*) with three characteristic average velocities, V_L^{Sup}, V_L^{Inf} and V_E (or V_S).

(5) For Zn-Al alloys with an Al content greater than 1 mass% but less than or equal to 5 mass%, if the solidification occurs from the base of the cylinder upward (one-directional vertical solidification upwards with heat losses from the top or three-interphase system) and the position vs. time curves grow monotonically only for the solidus interphase but not for the liquidus front, there are three solidification interphases, I_L^{Inf}, I_E and I_S running upwards, at temperatures T_L^{*Inf} and T_{Ei}^{*Inf} and T_{Ef}^{*Inf} (or T_S^{*Inf}), with three characteristic average velocities, V_L^{Inf}, V_E^{Inf} and V_S^{Inf}, and one solidification interphase I_L^{Sup} running downwards at temperature T_L^{*Sup}, with one characteristic average velocity V_L^{Sup}. If eutectic growth is initiated at the uppermost part of the probe, another interphase may be found running from the top to the bottom at an average velocity V_E^{Sup}. Note that if eutectic growth is considered, the three-interphase system shown in Fig. 7(c) may become a five-interphase system and five velocities can be determined.

(6) For Zn-Al alloys with an Al content less than or equal to 1 mass%, if the solidification occurs from the base of the cylinder upward and then two interphases [L/(S + L)] and [(S + L)/S] descend from the top towards the bottom of the cylinder (two-way one-directional solidification with four fronts of solidification), resulting in the presence of four interphases, two I_L^{Inf} and I_S^{Inf} going upwards with two characteristic average velocities V_L^{Inf} and V_S^{Inf} (or V_E^{Inf}), and two descending interphases, I_L^{Sup} and I_S^{Sup}, with velocities V_L^{Sup} and V_S^{Sup}. In this case, if eutectic growth occurs, two are I_L fronts, two are I_E fronts and two are I_S fronts at temperatures T_L^{*Sup}, T_{Ei}^{*Sup}, T_S^{*Sup}, T_L^{*Inf}, T_{Ei}^{*Inf} and T_S^{*Inf} with six characteristic average velocities, V_L^{Sup}, V_E^{Sup}, V_S^{Sup}, V_L^{Inf}, V_E^{Inf} and V_S^{Inf}. In this case, final solidification takes place somewhere inside the sample. Note that if eutectic growth occurs, the four-interphase system shown in Fig. 7(e) may become a six-interphase system and six different expressions for the velocities can be determined.

The experimental interphase average velocities as a function of distance determined for different experiences of Zn-base alloys are shown in Figs. 9(a) to (b). Figures 9(a) and (b) show the [L/(S + L)] and [(S + L)/S] interphase average velocities as a function of distance from one end of the specimen in the vertical case. Note that whereas for vertical solidification the distance is measured from the bottom to the top, for horizontal solidification the distance

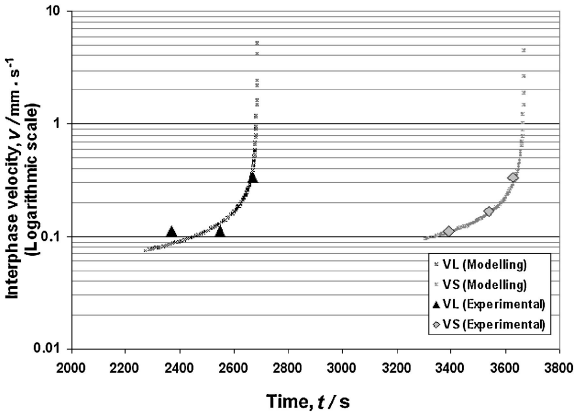

(a)

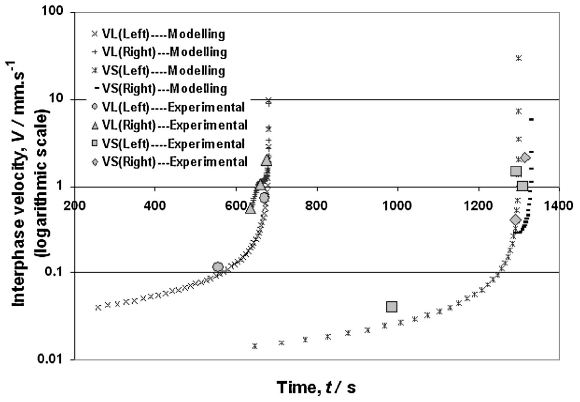

(b)

Fig. 10 Interphase velocity versus time for Zn-1%Al alloys. (a) Vertical solidification with a three-interphase system. (b) Horizontal solidification with a four-interphase system.

is measured from left to right. The experimental average velocities were determined from the distances between thermocouples and the time when the solidification began and concluded in each considered position.

The graphs of Fig. 10 show the interphase velocities versus time, determined from the experimental values and estimated from modeling using polynomial functions of time vs. distance when the solidification starts and ends in a given volume. The experimental average speed of the interphases in these experiments did not exceed 0.8 mm/s for vertical solidification, regardless of concentration or kind of interphase. However, in horizontal solidification, which extracts heat by the two ends, the experimentally determined maximum velocity for a specimen of Zn-1 mass%Al was about 2.1 mm/s for a liquidus interphase. In the case of two [L/(S + L)] interphases, the maximum velocity of the interphase was achieved at the time of the interphase collision, both having similar velocities. It is also important to mention that in a four-interphase system, by the time the interphase collision occurs, the average velocities of both interphases are usually different, whether they are [L/(S + L)] interphases collide or [(S + L)/S] interphases which collide.

As we have previously reported[16] for an Zn-2%Al alloy solidified in a vertical setup with only a two-interphase system running from the bottom to the top, the interphase velocities can be expressed as potential functions for both the speed of the [L/(S + L)] interphase and the speed of the [(E + L)/S] interphase. It was determined that the eutectic front velocity remains lower than the speed of the liquidus interphase, and as a result, the mushy zone increases rapidly. Furthermore, it was shown that there is a specific direction of motion of the interphases, which is only upward, indicating that caloric extraction is from the base and that nucleation of new equiaxed grains ahead of the columnar front is in a cascade mode. This behavior has been observed in other experiments with different concentrations.[8–10]

However, when three or four interphases were involved, the functions representing the velocity of the interphases were better expressed as exponential laws of the form:

$$\vec{v} = v_0 \cdot e^{(Ax^2+Bx)} \tag{1}$$

where:

v = interphase velocity [mm/s]

v_0 = characteristic constant velocity of the system, $v_0 = e^C$

A, B, C = determined experimental constants

x = position [mm]

Similar expressions can be determined in terms of time instead of position. It is noteworthy that the above expressions were determined for samples with a diameter of about 11 mm and probe lengths of about 150 mm.

Depending on the experiment, as determined in a given position, liquidus interphases may have velocities lower, similar, or greater than the solidus interphases. In most of the experiments involving columnar to equiaxed transition (CET), both interphases began at similar lower speeds, and then increased their speeds as a function of distance (measured from the chilled end). Usually, liquidus interphases increased their velocities at a higher rate than solidus interphases, and this situation induces an increase in the size of the mushy zone.

In a three-interphase system, the two liquidus interphases collide inside the sample, but the single solidus interphase moves from the bottom to the top, and it is there where solidification concludes. However, the point where liquidus interphases collide seems to be important in the formation of internal defects such as pores or holes.

From the experiments with four solidification interphases, which involved two ascending (I_L and I_S) and two descending interphases, the end of solidification happened inside the samples and it is in this position where the two solidus interphases which move in opposite direction do collide. Moreover, the two liquidus interphases running in opposite direction collide before the solidus interphases do, but the point of the collision is not (and generally should not be) the same point where the solidus interphases will meet. In a four-interphase system, at the instant of the collision of the liquidus interphases, the mushy zone increases its size abruptly, since two mushy zones are growing in both sides of a given sample. Besides, the collision of two S/(S + L) interphases indicates the final instant of solidification.

From the experiments conducted it can be seen that since the velocities of the interphases are not constant during the solidification process, there will be accelerations responsible for the change in the interphase velocities. Where possible, the upward and downward liquid and solidus interphase

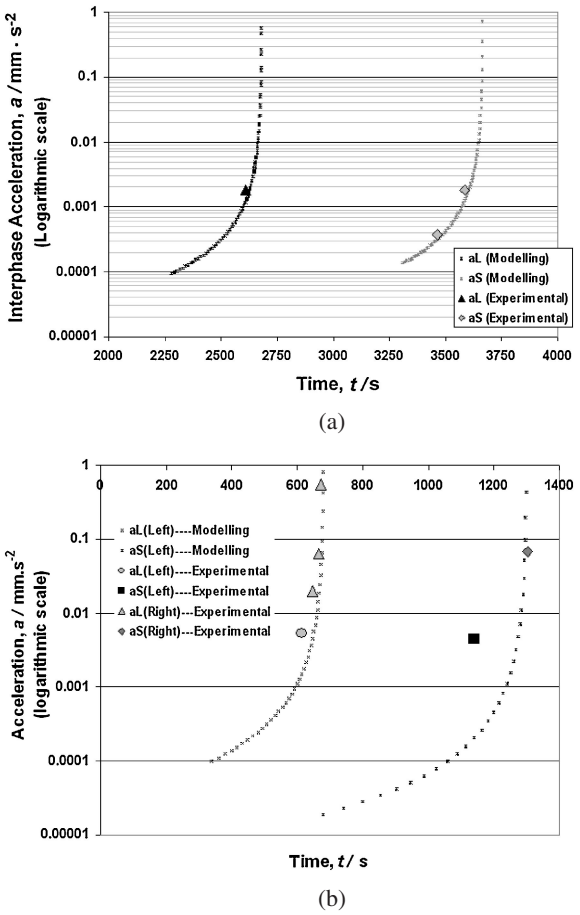

Fig. 11 Interphase acceleration versus time for Zn-1%Al alloys (absolute values). (a) Vertical solidification with a three-interphase system. (b) Horizontal solidification with a four-interphase system.

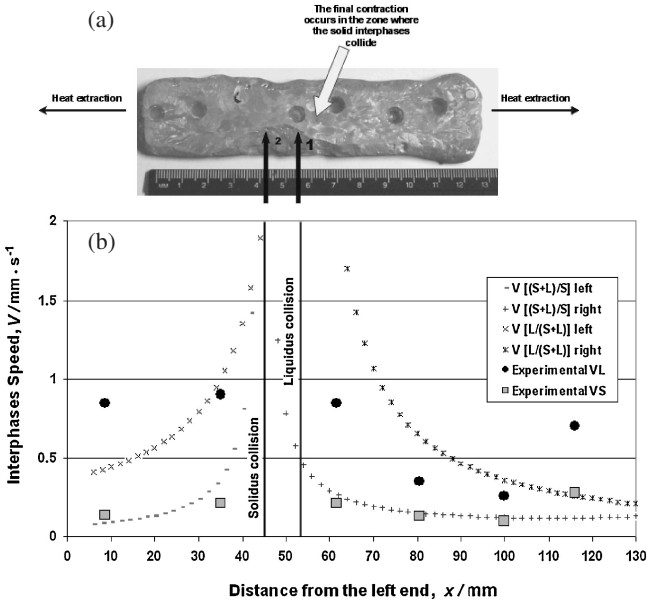

Fig. 12 (a) Sample horizontally solidified with four solidification interphases. (b) Velocity of the L/(S + L) and (S + L)/S interphases versus distance from one of the ends of the Zn-5 mass%Al alloy sample.

accelerations, a_L^{Inf}, a_L^{Sup} and a_S^{Inf}, a_S^{Sup} were determined for the various experiments. It can be seen from Figs. 11(a) and (b) that the accelerations of the interphases are not constant during the solidification process.

In a previous work,[16] for Zn-Al alloys solidified under similar conditions in a vertical setup but with a smaller probe diameter, the plot of ln (a) versus distance showed that the natural logarithm of the average acceleration as a function of the distance measured from the first thermocouple is almost linear and increases as the distance increases while the solidification progresses. From that dependence we derived an expression for the acceleration of the I_L and I_S upward and downward interphases:

$$\vec{a} = a_0 \cdot e^{(A_1 x)} \tag{2}$$

where:

a = interphase acceleration [mm·s^{-2}]
$a_0 = e^{B_1}$ = constant [mm·s^{-2}]
A_1 = constant [mm^{-1}]
x = position [mm]

The average acceleration increases exponentially as the solidification progresses.

Figure 11(a) shows that the maximum acceleration experimentally determined for the case of vertically solidified Zn-1 mass%Al alloys which presents a three-interphase system was less than 2×10^{-3} mm/s^2 for both interphases. The values of the maximum accelerations experimentally determined for the case of a specimen of Zn-1 mass%Al horizontally solidified (Fig. 11(b)) do not exceed 0.6 mm/s^2 for the [L/(S + L)] interphase and 0.07 mm/s^2 for the [(S + L)/S] interphase.

Figure 12 shows a horizontal directionally solidified Zn-5 mass%Al alloy with heat extraction from both ends of the sample, giving rise to four solidification interphases, I_L^{Left} and I_S^{Left} interphases moving to the right and I_L^{Right} and I_S^{Right} interphases moving to the left. Depending on the heat flux at each end, the velocities of the two [solid/(liquid + solid)] interphases are generally different in magnitude and have opposite direction and that the velocities of the [(liquid + solid)/solid] interphases are also different. As it can be seen from Fig. 12, for this particular setup and at a given position, the speed of the liquidus interphase is higher than the speed of the solidus interphase. It can also be noticed that the point where liquidus interphases collided (~53 mm) is not the same as the one where solidus interphases did (~45 mm), and that it is in this zone where the maximum contraction occurred.

For samples solidified horizontally in a one-directional setup with two cooling ways, we experimentally determined that the point where the two liquidus interphases collide is not in the same position as that where two solidus interphases do, due mainly to the disparity in the velocities and accelerations of the two opposite interphases undergoing interaction, in homogeneity and anisotropy of the mushy zone. The presence of four interphases determines that the end of the solidification occurs inside the cylindrical sample, being in this place where there is the greatest internal contraction. There are two characteristic points in the macrograph of Fig. 12: point #1, which is the location of the [L/(S + L)] interphase's meeting, and point #2, which is the location of the [S/(S + L)] interphase's meeting. Interestingly, it may be observed that the site of the largest contraction seems

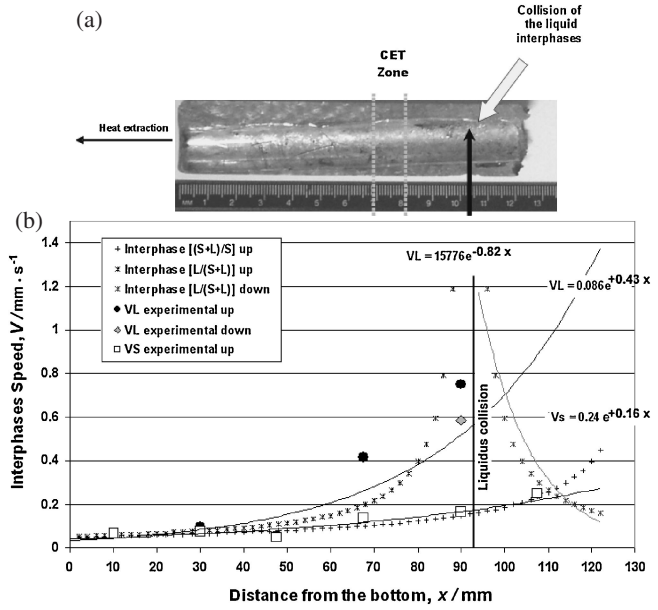

Fig. 13 (a) Macrograph indicating the position of the CET and the collision of the liquid interphases. (b) Curves of the $[L/(S+L)]$ and $[(S+L)/S]$ interphases as a function of the distance from the bottom. Zn-5 mass%Al alloy sample.

to occur where the liquidus interphases collided, probably because not enough liquid was available to fill the space.

The results obtained from the horizontal solidification were compared with those obtained for the same alloy composition, Zn-5 mass%Al alloys one-directional vertically solidified, with predominant heat extraction from the base (Figs. 13(a) and (b)). We detected the presence of three interphases, two I_L and one I_S, due to small heat losses from the top. The variation of the velocity of the $[L/(S+L)]$ interphase upward and downward and the changes in the velocity of the $[S/(S+L)]$ interphase for this type of solidification is shown in Fig. 13(b).

3.4 Temperature gradients

Figures 14(a) and 14(b) show temperature gradients determined as differences between two adjacent thermocouples for two Zn-Al eutectic alloys. One of the samples was horizontally solidified with two predominant paths of heat extraction and the other sample was vertically solidified with predominant heat removal from the base.

As seen in Fig. 14(a) for horizontal solidification cooling from both ends, the critical minimum gradient required to produce transitions from a CET structure in any portion of the specimen is not achieved at any moment, as revealed by the sample macrograph shown in Fig. 4(b). Figure 14(b) shows the temperature gradients versus time for Zn-5 mass%Al directionally solidified alloys in a vertical setup. The critical minimum gradient required to produce transitions from a CET structure is achieved, as revealed by the sample macrograph shown in Fig. 13(a).

Figure 15(a) shows the minimal temperature gradients as a function of distance from the bottom of the Zn-5 mass%Al alloy sample horizontally solidified. It can be seen that in spite of there are two minimum gradients, is not achieved at any moment the critical minimum gradient required to

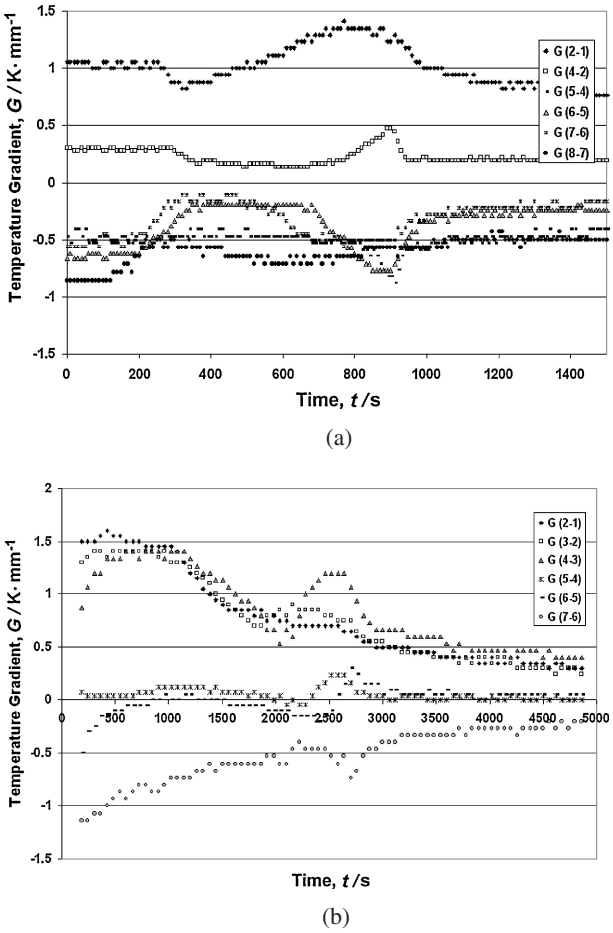

Fig. 14 Temperature gradients versus time for Zn-5 mass%Al directionally solidified alloys in (a) a horizontal and (b) a vertical setup.

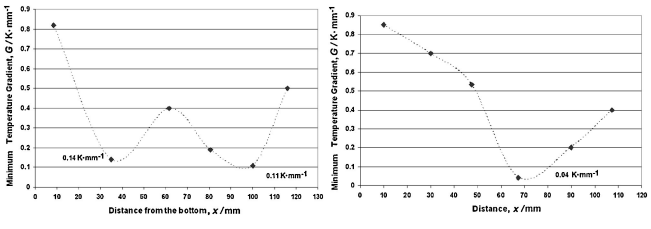

Fig. 15 Minimal temperature gradients as a function of distance from the bottom of the Zn-5 mass%Al alloy sample. (a) Horizontally: the critical minimum gradient required to produce the CET in any portion of the specimen is not achieved at any moment. (b) Vertically: There are sections of the vertical samples with a minimum and critical gradient that enable a CET.

produce the columnar to equiaxed transition structure (CET) in any portion of the specimen. Figure 15(b) shows that there are a section of the vertical cylindrical probe with a lower temperature gradient and this gradient has a critical and minimum value. Thus, in these conditions, a columnar-equiaxed transition structure (CET) did occur.

As observed in Fig. 15, the horizontally solidified specimen (a) shows the existence of two minimum gradients, one at 35 mm and another at 100 mm. However, the values of these gradients do not reach the minimum values ahead of the interface structure to produce transitions, and thus the

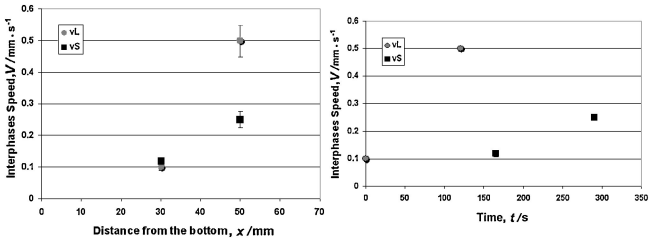

(a) (b)

Fig. 16 Interphase velocities as a function of (a) distance and (b) time for a Zn-2 mass%Ag alloy directionally solidified using a vertical solidification system with two interphases.

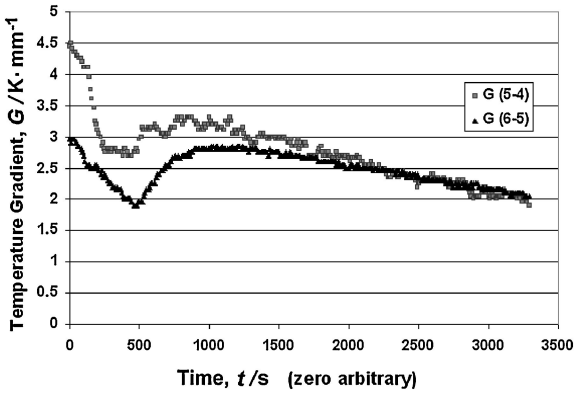

Fig. 17 Temperature gradients as a function of time for a Zn-2%Ag alloy directionally solidified using a vertical solidification system with two interphases.

structure was fully equiaxed. The vertically solidified specimen show in Fig. 15(b) reaches an absolute minimum gradient value of 0.04 K·mm^{-1} at 67.5 mm from the bottom. The start of the CET of the specimen was observed at 65 mm, and the ending of the CET area was located at 88 mm from the bottom.

The interphases velocities as a function of distance and as a function of time for a Zn-2 mass%Ag alloy directionally solidified are shown in Figs. 16(a) and (b) respectively. The alloy sample was solidified in the vertical setup, having only a two-interphase system. Although this kind of alloys may go through a peritectic reaction if the alloy concentration increases locally, it can be seen from the figure that the liquidus interphase began nearly at the same speed as the solidus front, and, as the solidification progresses, the liquidus interphase moves at a faster rate than the solidus interphase. The experimental velocities determined for this system are of about the same order of magnitude as those determined for vertically solidified Zn-Al alloys. However, it was noticed that in the Zn-Ag system in the diluted region, liquidus interphases increase their temperatures as the solidification progresses.

Figure 17 shows the time evolution of the temperature gradients experimentally determined for the Zn-2%Ag alloys vertically solidified with a two interphases system. As it can be seen, since the minimum critical gradient is not reached at any time in the sample, no evidence of CET is expected.

4. Conclusions

The main conclusions of this research are that:

(1) The solidification kinetics was found to be different when comparing the horizontal one-directional solidification with two pathways of heat extraction with the vertical one-directional solidification with a prevailing path of heat extraction.

(2) In a three or four interphase system and for both types of solidification (horizontal and vertical), liquidus interphases may collide in a position different from that of the solidus or eutectic interphases.

(3) In the solidification experiments conducted and for the conditions here imposed, the velocity of the liquidus interphase is usually greater than or sometimes equal to the velocity of the solidus or eutectic interphases.

(4) In the collision area of the solidus interphases, the final contraction which can cause cavities, pores and internal defects, occurs.

(5) When reaching critical minimum gradients greater than 0.1 K/mm, the CET did not occur in the horizontal one-directional solidification with a four-interphase system.

Acknowledgments

The authorswould like to thank CONICET for the financial support. The work was partially granted by BID 1728/OC-AR-PICT-O N° 36866. Also, thanks are given to chemical engineering students Adriana Candia and Alejandro Barbaro for their collaboration in the realization of the experiments.

REFERENCES

1) B. Chalmers: *Principles of Solidification*, (John Wiley & Sons, New York, 1964) pp. 5–19.
2) W. Kurz and D. J. Fisher: *Fundamentals of Solidification*, (Trans. Tech. Publications, Aedermannsdorf–Switzerland, 1986) pp. 21–64.
3) S. C. Flood and J. D. Hunt: *Metals Handbook*, Edition 9[a], Chapter 15, Casting, (American Society for Metals, Ohio, 1988) pp. 130–136.
4) J. A. Spittle: Int. Mater. Rev. **51** (2006) 247–269.
5) S. Robles Casolco: *Caracterización Mecánica del Eutectoide Zn-Al modificado con Plata*, (Universidad Nacional Autónoma de México, México, 2004) pp. 12–36.
6) H. E. Boyer and T. L. Gall: *Metals Handbook*, (Desk Edition, American Society for Metals, USA, 1990) pp. 18–19.
7) M. Sahoo and L. V. Whiting: AFS Trans. **92** (1984) 861–870.
8) A. E. Ares and C. E. Schvezov: Metall. Mater. Trans. A **31** (2000) 1611–1625.
9) A. E. Ares, S. F. Gueijman, R. Caram and C. E. Schvezov: J. Crystal Growth **275** (2005) e319–e327.
10) A. E. Ares and C. E. Schvezov: Metall. Mater. Trans. A **38** (2007) 1485–1499.
11) G. Kehl: *Fundamentos de la Práctica Metalográfica*, (Aguilar, Madrid, 1963) pp. 25–37.
12) C. A. Gandin: ISIJ Int. **40** (2000) 971–979.
13) I. Ziv and F. Weinberg: Metall. Mater. Trans. A **20** (1989) 731–734.
14) M. A. Martorano, C. Beckermann and C. A. Gandin: Metall. Mater. Trans. A **34** (2003) 1657–1674.
15) S. F. Gueijman, A. E. Ares and C. E. Schvezov: 8° Congreso Internacional de Metalurgia y Materiales. CONAMET/SAM 2008, ed. by Sociedad Chilena de Metalurgia y Materiales-Asociación Argentina de materiales, (Santiago de Chile, 2008).
16) S. F. Gueijman, A. E. Ares and C. E. Schvezov: 3° Congreso Latinoamericano de Fundición. COLFUN'07, ed. by Cámara Argentina de Fundidores, (Tandil, 2007) pp. 1–16.